1990-2016 surface solar radiation variability and trend over the Piedmont region (northwest Italy)

Veronica Manara (v.manara@isac.cnr.it)

Institute of Atmospheric Sciences and Climate, ISAC-CNR, Bologna, Italy

Manuela Bassi (manuela.bassi@arpa.piemonte.it)

Department of Forecasting Systems, Regional Agency for Environmental Protection of Piedmont, Turin, Italy

Michele Brunetti (m.brunetti@isac.cnr.it)

Institute of Atmospheric Sciences and Climate, ISAC-CNR, Bologna, Italy

Barbara Cagnazzi (b.cagnazzi@arpa.piemonte.it)

Department of Forecasting Systems, Regional Agency for Environmental Protection of Piedmont, Turin, Italy

Maurizio Maugeri (maurizio.maugeri@unimi.it)

Department of Environmental Science and Policy, Università degli Studi di Milano, Italy; Institute of Atmospheric Sciences and Climate, ISAC-CNR, Bologna, Italy

Corresponding author: Veronica Manara, Institute of Atmospheric Sciences and Climate, ISAC-CNR, via Gobetti 101, 40129, Bologna, Italy (v.manara@isac.cnr.it) http://orcid.org/0000-0001-9652-4228

Abstract

A new surface solar radiation database of 74 daily series is set up for the Piedmont region (northwest Italy) for the 1990-2016 period. All the series are subjected to a detailed quality control, homogenization and gap-filling procedure and are transformed into relative annual/seasonal anomaly series. Finally, a gridded version (0.5°x0.5°) of the database is generated. The resulting series show an increasing tendency of about +2.5% per decade at annual scale, with strongest trend in autumn (+4% per decade). The only exception is winter, showing a negative but not significant trend. Considering the plain and mountain mean series, the trends are more intense for low than for high elevations with a negative vertical gradient of about -0.03% per decade per 100m at annual scale and values up to -0.07% per decade per 100m in spring.

Focusing on clear days only (selected by CMSAF-COMET satellite data over the 1991-2015 period), trend significance strongly increases and both low and high elevation records exhibit a positive trend in all seasons. However, the trends result slightly lower than for all-sky days (with the only exception of winter). The differences observed under clear-sky conditions between low and high elevations are more pronounced in winter, where the trend shows a negative vertical

gradient of about -0.1% per decade every 100m.

Overall, this paper shows how a high station density allows, performing a more detailed quality control thanks to the higher performances in detecting the inhomogeneities with higher data availability and capturing regional peculiarities otherwise impossible to observe.

1. Introduction

The fraction of solar radiation that reaches the Earth's surface (surface solar radiation - $E_{g\downarrow}$) is the primary energy source for the Earth's climate system governing a large number of physical and chemical processes (Stanhill 1983; Stephens et al. 2012; Wild 2016). Any possible variation is important not only for scientific interests, but it has a lot of implications for example for agricultural production and solar power generation (Stanhill 1983; Wild et al. 2015). While, it is widely recognized that $E_{g\downarrow}$ decreased between the 1950s and the 1980s of about 3-9Wm^{-2} ("Global dimming"), and increased since the 1980s of about 1-4Wm^{-2} ("Brightening period") (Wild 2009), it is a debate whether these variations are caused by aerosols or cloud effects, even if they are not completely independent (Twomey et al. 1984; Albrecht 1989; Ramanathan et al. 2001; Lohmann and Feichter 2005). Uncertainties are mainly connected to the lack of a full knowledge of all the mechanisms that influence $E_{g\downarrow}$ variability. As far as ground-based observations are concerned, the main problem is connected to the low availability both of $E_{g\downarrow}$ and aerosol/cloud long-term quality-checked data (Wild 2009). Some of the studies reported in literature point to the dominant role of aerosols (e.g., Norris and Wild 2007; Ruckstuhl et al. 2008; Turnock et al. 2015), while other studies show how cloud effects are more dominant contributors to $E_{g\downarrow}$ variations (e.g., Mateos et al. 2014; Kambezidis et al. 2016; Boers et al. 2017; Tang et al. 2017; Pfeifroth et al. 2018), depending on the considered region and period. In particular, over the Mediterranean area, a recent study (Kazadzis et al. 2018) analyzing a long-term series of $E_{g\downarrow}$ in Athens (Greece) suggests that observed $E_{g\downarrow}$ variations can be only partly attributed to cloudiness and are mostly caused by aerosol load changes. The same result was obtained for the same area by Founda et al., (2014) starting from sunshine duration data, especially during the brightening period. Similar results are obtained for Switzerland by Sanchez-Lorenzo and Wild (2012), who attributed the major part of the observed decadal variability until the early 1980s to clouds, suggesting however that aerosols explain the strong brightening detected in the subsequent period. Differently, Mateos et al., (2014) attributed three fourths of the observed increasing tendency after the 1980s in Spain to reductions in total cloud cover and only one fourth to the reduction of the columnar aerosol load. As far as Italy is concerned, Manara et al., (2015), comparing sunshine duration and total cloud cover series, hypothesized the importance of other factors, like aerosols, in addition to cloudiness, to completely explain the observed sunshine duration trends especially during the dimming period. Over the same area, Manara et al. (2016a) went more in depth setting up and analyzing a new homogenized dataset of 54 surface-

based $E_{g\downarrow}$ records over the period 1959-2013. They analyzed trends both under all-sky and clear-sky conditions, obtaining stronger tendencies under clear-sky than under all-sky conditions in all seasons during the dimming period, and in winter and autumn during the brightening period. They suggest that $E_{g\downarrow}$ variability is due both to natural (especially in the south) and anthropogenic (especially in the north) aerosol variations under clear-sky conditions and that cloud cover variations have partially masked the signal due to aerosol variations under all-sky conditions.

The dataset of Italian long $E_{g\downarrow}$ records has however some limitations including a wide fraction of missing data (Manara et al. 2016b), the lack of high-elevation sites and a poor coverage over the Italian alpine region. It is therefore very important to increase the data availability by merging the national $E_{g\downarrow}$ dataset (Manara et al. 2016a) with data recovered by the regional services. Networks of these services have data only since the beginning of the 1990s. However, a high station density, allows at first a more accurate quality control of the series (Brunetti et al. 2006) and then, gives the possibility to better study the spatial variability of the $E_{g\downarrow}$ signal and to investigate more in depth local effects (e.g., differences among low and high elevations, and among rural and urban areas).

Piedmont is a region in the northwest of Italy (44°03' - 46°27'; 6°37' - 9°12'), close to the Mediterranean Basin, an area of particular interest in the context of climate change for the different types of aerosols that accumulate there (e.g., sea salt aerosols from the Mediterranean Sea and the Atlantic Ocean, pollution aerosols from Europe, dust from the Sahara Desert and biomass burning aerosols from Eastern Europe (Georgoulias et al. 2016)). Moreover, its territory is of particular interest including both a part of the Po Valley, one of the most polluted areas in Europe (Bressi et al. 2016), and a part of the Alpine chain allowing investigating the possible differences between $E_{g\downarrow}$ variations at low and high altitudes (Marty et al. 2002; Sanroma et al. 2010).

In this context, this study aims at collecting, quality-checking and analyzing for the first time a high-density $E_{g\downarrow}$ database for the Piedmont area for the period 1990-2016. Specifically, Section 2 describes the data pre-processing, from the raw daily series to the seasonal and annual gridded anomaly series both under all- and clear-sky conditions, Section 3 presents the obtained results, and Section 4 discusses the results and gives some conclusive remarks.

2. Data Pre-processing

2.1 Data

The $E_{g\downarrow}$ database analyzed in this work (see Figure 1a) is composed of 74 daily series over the period 1990-2016. The most part of them (60 series) are recovered from the regional service of the Piedmont Area (Arpa Piemonte - http://www.arpa.piemonte.gov.it/), while a small part (14 series) are recovered from other sources: 2 series come from the National Agro-Meteorological Database (BDAN – Banca Dati Agrometeorologica -

http://cma.entecra.it/homePage.htm), 1 series from the Italian Air Force (AM - Aeronautica Militare Italiana – http://clima.meteoam.it/istruzioni.php), and 11 series from Switzerland (MeteoSwiss - http://www.meteoswiss.admin.ch/home.html). We have decided to use 2 series of the Piedmont region already considered by Manara et al. (2016a) and other series from neighboring areas both to give a full representation of the $E_{g\downarrow}$ data availability in this region and to increase the information in the boundary areas to provide more robust trend estimate for those grid-points located at the border (see Section 2.6).

Some of the series that do not come from the Piedmont regional service were already analyzed by Manara et al. (2016a), however, here the raw series are used and the quality-control and homogenization analysis are applied again in the light of the higher data availability in the dataset under analysis.

The data that come from the Piedmont regional service are recorded with a HE20K CAE – radiometer or with an AB20/K CAE first-class albedometer (WMO - ISO9060), while for the other series different types of radiometers are used (see Manara et al. (2016a) for details). The calibration of the radiometers is periodically checked (one or two times per year) by means of a reference instrument and when a problem is found the instrument is substituted.

Overall, the mean minimum distance among stations is about 13km and 63.5% of the stations are located in the plain area (elevation lower than or equal to 600m), while 36.5% are located in the mountain area (elevation higher than 600m) (Figure 1b). The station with the highest elevation is Capanna Margherita located at 4560m.

The quality of the series is checked in two steps. At first, all the daily series are subjected to preliminary quality controls in order to remove gross errors (e.g., values equal to or lower than zero and values higher than the corresponding extra-terrestrial radiation) and then all the series are subjected to a homogenization procedure in order to eliminate non-climatic signals (see Section 2.4).

The temporal evolution of the average number of available series (Figure 1c) shows that the best data availability concerns the 2003-2016 period. Moreover, the common variance between two stations decreases with increasing distance as expected (Hakuba et al. 2013; Schwarz et al. 2017) reaching, for the daily series, a value of 50% at about 90km.

2.2 Gap-filling of the daily series

All the months with less than 50% of available daily data (they are less than 1% of the months with at least one datum) are not included in the analysis. For all the other months (i.e., all months with more than 50% of available data), each missing daily value (*daily-t*) is estimated by means of the most correlated reference series using Equation 1, based on the assumption of the constancy of the ratio between test (*t*) and reference (*r*) series:

$$E_{g\downarrow daily-t} = E_{g\downarrow\, daily-r} \overline{E_{g\downarrow common\ days-t}} \Big/ \overline{E_{g\downarrow common\ days-r}} \quad (1)$$

One series is considered a "good" reference series if the missing value in the test series is available (*daily-r*) and it belongs to same area of the test station (plain – elevation lower than/equal to 600m or mountain – elevation higher than 600m). Moreover, the correlation between the test and the reference series in the month that includes the considered missing daily value must be at least 0.70 (i.e., the common variance must be at least about 50% (Auer et al. 2005)). If the station belongs to the plain area, the distance between test and reference series must be less than 50km in order to not transfer the signal of local effects (e.g., fog) from a station to another one. Finally, test and reference series must have at least 12 (10 for February) daily values in common (*common days)* in the considered month..

The percentage of available data before the daily gap-filling was about 97% (where the percentage is calculated considering the period of activity of each station), and this procedure allowed estimating about 2% of data increasing the data availability to about 99%.

The procedure is validated using the leave-one-out approach (each value is supposed as missing and estimated with the procedure explained above) and more than 80% of the ratios between observed and estimated values are comprised between 0.8 and 1.2. This value increases to near 90% if only the series located in the plain area are considered.

2.3 Estimation of the monthly series

After the procedure applied in Section 2.2, all the monthly values are calculated as arithmetic mean if all the daily values are available in the corresponding month. For those months, which are not complete, but with a good reference series available, Equation 2 is used to adjust the monthly arithmetic mean to take into account the contribution of those days that are missing.

$$\overline{E_{g\downarrow corrected-t}} = \overline{E_{g\downarrow all\ days-r}}\, \overline{E_{g\downarrow common\ days-t}} \Big/ \overline{E_{g\downarrow common\ days-r}} \quad (2)$$

The reference series is selected as explained in Section 2.2, but in this case the corresponding month in the reference series must be complete (*all days-r*). Finally, if there is not a good reference series, the monthly mean is calculated the same as arithmetic mean only if at least 80% of the daily observations are available.

After the procedures explained in Section 2.2 and 2.3, all the series have at least 10 years of available data over the period 1990-2016, with the highest data availability after 2003 (more than 60 records per year).

2.4 Homogenization

As second step of the quality control procedure (see Section 2.1), all the monthly series were subjected to a

homogenization procedure in order to identify and remove non-climatic signals (Aguilar et al. 2003; Brunetti et al. 2006). Specifically, in this procedure, each test series is compared against "candidate" reference series in sub-groups of 10 series, by means of the Craddock test (Craddock 1979). The "candidate" reference series are chosen in the same area and with similar elevation in order to avoid exporting the signal of a region into another one. For each couple of series (test and "candidate" reference series) the cumulative normalized differences between test and "candidate" reference series are calculated (Manara et al. 2017a) and the breaks in the test series are identified by changes in the slope of this series. In particular, in order to be sure that the observed breaks are ascribable to the test series, only the breaks highlighted by more than one "candidate" reference series are considered for the correction. Then, the adjustment factors are calculated using only the "candidate" reference series that prove to be homogeneous (note that the homogeneity test has been applied to all the series) in a sufficiently long period centered on the break. In particular, the length of the period is selected as the longest period centered on the break for which all the selected reference series are homogenous. Finally, a daily version of the adjustment factors is also generated in order to homogenize the daily series too. The advantage to use more than one reference series and series that come from different networks is that this allows identifying also inhomogeneities due to synchronous changes that affect the whole network, otherwise not detectable by relative tests.

The adopted technique is based on an indirect methodology (relative homogeneity test based on statistical methods), even if great attention has been paid to metadata (Aguilar et al. 2003; Manara et al. 2017c). In fact, comparing the detected breaks with the corresponding ARPA metadata available for the 2003-2016 period, we found that about 43% of the identified breaks corresponds to documented changes in instruments, which is one of the main source of inhomogeneities.

Figure 2 shows the average annual $E_{g\downarrow}$ anomaly series (relative anomalies with respect to the 1990-2016 mean) before and after the homogenization procedure together with the corresponding Gaussian low-pass filters (the details on how the regional $E_{g\downarrow}$ anomaly series is obtained will be explained in the following sections). The mean annual adjustment series (blue line in Figure 2), obtained by averaging the mean annual adjustments over all single records, shows that in the 1990-2007 period, the mean series has been increased by about 1%, while during the following 2008-2015 period, it has been subjected only to very small changes. This is because in the homogenization procedure, the period before a break is generally adjusted to the more recent period to facilitate future updating of the dataset. Overall, the adjustment factors (figure not shown) range between 0.681 and 1.293 even if these high values concern only single years and single series. It is interesting to note that 13 series did not highlight any break and did not require any adjustment.

After the homogenization procedure, the common variance at monthly scale decreases to 50% at about 110km. The mean common variance decreases at a higher distance if only the plain series are considered showing a value of 50% at

215km. Lower values are obtained for the mountain series because of less robust statistic for short distances due to the lower number of available series (Schwarz et al. 2017). However, the mean variance for all the subsets of series (Piedmont, plain and mountain) at 50km is comprised between about 50% and 80%.

2.5 Gap-filling and anomaly series

Once the series are homogenized, the remaining gaps over the whole 1990-2016 period are filled in the monthly series. Specifically, each reconstructed monthly value is obtained as the median of a set of five estimated values, calculated under the assumption of the constancy of the ratio between incomplete and reference series, where the reference series are selected as explained in Section 2.1 and 2.2 with the additional constrain that the reference and test series should have in common at least 5 values for the considered month.

After the gap-filling, all the series have at least 97% of available data over the 1990-2016 period with the only exception of Milano Linate. The procedure is validated using the leave-one-out approach and about 95% of the ratios between observed and estimated values are comprised between 0.9 and 1.1.

Then, all the series are transformed into seasonal and annual relative anomaly records with respect to the 1990-2016 mean. Specifically, seasons are defined according to the scheme December-January-February, March-April-May, June-July-August, September-October-November and winter is dated according to the year in which January and February fall. According to this scheme, the year is defined as the December-November period.

2.6 Gridding

Finally, a gridded version of the seasonal and annual $E_{g\downarrow}$ anomaly series is generated in order to balance the contribution of those areas with a higher number of stations with those that have a lower station coverage. A grid of 0.5°x0.5° resolution is constructed with an Inverse Distance Weighting approach as described by Brunetti et al. (2006), with the addition of an angular term to take into account the anisotropy in the spatial distribution of the stations. Specifically, a seasonal/annual gridded value is calculated if there is at least one series at a distance lower than or equal to *d/2*, or at least two series at a distance lower than or equal to *d*, where *d* is defined as the mean distance from one grid-point to the next one calculated overall adjacent points of the grid and is here equal to about 68km. The resulting grid consists of 20 grid-points (see Figure 1a). Moreover, for each grid-point a representative elevation is estimated as weighted mean (using the same weights discussed above) of the elevations of the involved stations. 8 grid-points are located in the plain area (weighted elevation lower than or equal to 600m), while 12 grid-points are located in the mountain area (weighted elevation higher than 600m) (Figure 1a).

Finally, the regional annual and seasonal $E_{g\downarrow}$ anomaly series for the Piedmont area is obtained averaging all the annual and seasonal anomaly grid-point series. Moreover, one series representative of the plain and one of the mountain areas are obtained averaging the plain and mountain annual and seasonal anomaly grid-point series, respectively.

2.7 Clear-sky series

Starting from the homogenized daily series presented in Section 2.4, we aimed at determining clear-sky $E_{g\downarrow}$ series. Being cloud cover data not available for the stations' network used in the present work, the cloud cover information used as reference to select the clear days come from the CM SAF ClOud Fractional Cover dataset from METeosat First and Second Generation – Edition 1 (COMET - Stockli et al. 2017). These data are available for the 1991-2015 period at daily scale with a resolution of 0.05°x0.05°.

Specifically, for each station, we selected those $E_{g\downarrow}$ days for which the corresponding CFC (Cloud Fractional Cover) value in the nearest grid-point was lower than or equal to 12.5% (equivalent to 1 okta) (following the same criteria of Manara et al. 2016a). In particular, the mean distance between each station and the central point of the selected grid-cell is about 2km with an average fraction of clear-sky days per station equal to about 23%.

Then, we obtained the Piedmont plain and mountain relative anomaly series (with respect to the 1991-2015 period), as already explained in Section 2.5 and 2.6 for the all-sky conditions. Moreover, to take into account the possibility that the clear-sky records may contain only a small number of days (as already explained by Manara et al. (2017b)), and so monthly averages may be influenced by the dates in which these days fall, we transformed the daily $E_{g\downarrow}$ data into clearness index data removing in this way the influence of the solar zenith angle. Then, the corresponding monthly means were retransformed into absolute records using the exo-atmospheric value relative to the central day of the corresponding month.

3. Results

3.1 All-sky $E_{g\downarrow}$ variability and trends

The annual and seasonal Piedmont regional series are shown in Figure 3 with the corresponding filters (11-year window, 3-year standard deviation Gaussian low-pass filter). The slope of the trends, estimated using the Theil-Sen method (Theil 1950; Sen 1968), together with the significance, estimated using the Mann-Kendall non parametric test (Sneyers 1992), are shown in Table 1.

The annual series shows a statistically significant (p-value ≤ 0.05) increasing tendency of about +2.5% per decade over the 1990-2016 period. Moreover, the trend is positive and significant (p-value ≤ 0.1) in all seasons with the only

exception of winter, where the trend is negative (more intense after the beginning of 2000s) even if not statistically significant over the considered period. The most intense increase is observed in autumn (about +4.0% per decade) and in summer (about +2.7% per decade).

Considering the spatial distribution of trends (Figure 4), it is possible to observe how, at annual scale, the trends are positive and significant (p-value ≤ 0.1) over the whole region, and become stronger moving from the Alps toward the Po plain.

At seasonal scale, autumn is the only season that shows a statistically significant trend (p-value ≤ 0.1) for all the grid-points, with higher values than the other seasons (especially for the grid-points located in the south-east). During spring, not all the grid-points show a significant trend and the grid-points located in the mountain area show lower values than those located in the plain area. Differently, during summer, a well-defined spatial pattern is not evident, and during winter all the grid-points show a negative but not significant trend.

Even if the differences are not always statistically significant, it is worth mentioning that trends, when significant, are stronger for the plain area than for mountain area (Table 1), with the only exception of summer, where the trend is slightly higher in the mountain area than in the plain area. Overall, at annual scale the increase is about +2.6% and +2.3% per decade (p-value ≤ 0.05) for the plain and mountain areas, respectively. At seasonal level, the most evident differences between plain and mountain areas are evident in spring where the trend of the ratio between plain and mountain series is +0.7% per decade (p-value ≤ 0.05 - Table 1), underlying how the trend is stronger in the regions with low elevation with respect to the region with high elevation. This is confirmed also by the variation of the trend intensity with the elevation (Figure 5), which shows that the trend intensity decreases of about -0.07% per decade (p-value ≤ 0.05) every 100m of increase in elevation. The decrease of the trend intensity is evident especially for those grid-points located at elevation higher than 700-1000m (Figure 5). A similar behavior is observed also at annual scale, where the trend of the ratio between plain and mountain series is about +0.4 (p-value ≤ 0.1) and the trend intensity decreases of about -0.03% per decade (p-value ≤ 0.05) every 100m of increase in elevation (see Table 1 and Figure 5).

This different behavior between high and low elevation was not observed by Manara et al. (2016a) because of the lack of available information above 600m. This highlights the importance of a dense network to better resolve the spatial pattern in $E_{g\downarrow}$ variability. However, from a comparison between the annual Piedmont plain series presented in this paper and the annual mean anomaly series (northwest Italy), obtained averaging the grid-point series (available over the 1959-2013 period) from Manara et al. (2016a) belonging to the area under analysis the agreement is very good (Figure 6). The two series show a correlation of 0.84 over the common period (1990-2013), and 0.88 over the period selected as reference to calculate the anomalies (1990-2004) in spite of the very poor data availability for northwest Italy in Manara et al. (2016a). The merging of the Manara et al. (2016a) northwest Italy series with the Piedmont plain record (see

Figure 6) provides therefore an indication of Piedmont $E_{g\downarrow}$ variability on longer time scales, even though there is larger uncertainty before 1990.

The trends over the common period (1990-2013) show an increase of about +3% and +5% per decade (p-value ≤ 0.05) for the Piedmont plain and the northwest Italy series obtained from Manara et al. (2016a), respectively. These differences are mostly due to two main factors: i) the existence of a west-east intensification of the trend (see Figure 4), causing stronger trends in the Manara et al. (2016a) derived record, as it is mostly influenced by stations located to the east of Piedmont; ii) the influence of some Swiss stations that exhibit an inhomogeneity around 2005 due to the introduction of a new type of radiometer in the whole Swiss network (Suter et al. 2006). This break was only partly corrected in the Manara et al. (2016a) data set due to the very poor availability of Italian data in the northwest and in the alpine region. Differently, it was easier detecting and adjusting it with the very high data availability of the new Piedmont database. This is an interesting example of the benefit of datasets with records from different networks: it may in fact happen that within one specific network there are inhomogeneities that affect all the stations at the same time (or at least most of them) and can therefore not be detected by means of relative homogenization methods (if only records from that network are available).

3.2 Clear-sky $E_{g\downarrow}$ variability and trends

The annual and seasonal Piedmont regional series obtained under clear-sky conditions are shown (red lines) in Figure 7 with the corresponding filters (11-year window, 3-year standard deviation Gaussian low-pass filter). The filters (black lines) under all-sky conditions are shown too. Note that in order to better compare the results, all the values presented in this section (both for clear and all-sky conditions) refer to the 1991-2015 period and the anomalies are calculated with respect to this period.

Removing the cloud contribution, the interannual variability (standard deviation of the residuals of the series from the low-pass filters) strongly decreases with respect to all-sky conditions with values lower than 0.02 in all seasons. As a consequence, trend significances strongly increase.

Clear-sky records trends are positive and highly significant (p-value ≤ 0.001) in all seasons (Figure 7). Trends result however slightly lower with respect to all-sky conditions (about +2.3% and +2.75% per decade at annual scale under clear-sky and all-sky conditions, respectively) with the only exception of winter, where the all-sky record trend is negative (but not significant), whereas the clear-sky record trend is positive and highly significant (about +3.2% per decade - p-value ≤ 0.001). This behavior is confirmed also analyzing separately the plain and the mountain regional series: in both cases the strongest increase is found (differently from all-sky conditions) in winter (about +4.1% and +2.9% per decade for the plain and mountain area, respectively - p-value ≤ 0.001). Moreover, under clear-sky

conditions winter is the season with the most evident difference in trends between plain and mountain area (Figure 8). In particular, the ratio between the two regions shows a significant (p-value ≈ 0.01) increasing tendency of about +1% per decade, resulting from a stronger increase for low than for high elevations, and the trend intensity shows a negative trend of about -0.1% per decade per 100m of elevation (p-value ≤ 0.001).

4. Discussion and conclusions

One of the main sources of uncertainty in understanding the causes underlying surface solar radiation ($E_{g\downarrow}$) variability observed over the last decades in most regions of the world is connected to the availability of a low number of long-term quality checked series. Moreover, very often also in the regions where they are available, they do not have the necessary spatial resolution to study in depth local effects.

Recently, a new dataset of 54 series has been set up over the Italian territory for the 1959-2013 period (Manara et al. 2016a). On one side, this dataset gives important information on how $E_{g\downarrow}$ has changed; on the other side, it has some limitations including a wide fraction of missing data and the lack of high-elevation sites. In this context, a new $E_{g\downarrow}$ database, composed of 74 daily series for the 1990-2016 period (Figure 1), is set up for the Piedmont region, in the northwest part of Italy. 63.5% and 36.5% of the stations are located in the plain and mountain area respectively (elevation lower than or equal to/higher than 600m), with an overall minimum mean distance among stations equal to about 13km. After a detailed quality control of the daily series, the corresponding monthly series are subjected to a homogenization procedure (Figure 2) by means of the Craddock test (Craddock 1979). From a comparison between the detected breaks and the available metadata recovered from the Piedmont regional service (for the 2003-2016 period), it resulted that about 43% of them corresponds to changes in instruments, underlying how homogenization is mandatory to obtain reliable climatic time series. Then, after the gap-filling procedure, all the series are transformed into relative annual/seasonal anomaly series (with respect to the 1990-2016 period) and interpolated over a regular grid (0.5°x0.5°).

The resulting Piedmont mean series, obtained under all-sky conditions (Figure 3 – Table 1), show an increasing tendency over the whole considered period of about +2.5% per decade at annual scale. The increasing tendency is in agreement with the "brightening period" reported in literature even if a wide range of values is reported depending on the considered region and period (Wild 2009, 2016; Sanchez-Lorenzo et al. 2015). At seasonal scale, the strongest increase is in autumn, with a trend of about +4% per decade, and only winter presents negative trend even if not significant. Considering the plain and the mountain mean series separately (grid-points with an equivalent weighted elevation lower than or equal to/higher than 600m respectively), the trends (Figure 4 – Table 1) are stronger for low than for high elevations, with the ratio between plain and mountain series showing at annual scale a trend of +0.4% per decade, with an estimated vertical gradient of the trend of about -0.03% per decade every 100m. At seasonal scale, this

difference is more pronounced during spring, where the ratio between plain and mountain series shows an increasing tendency of about +0.7% per decade, with a vertical gradient of the trend of about -0.07% per decade per 100m.

Removing the cloud contribution from the $E_{g\downarrow}$ series (for the 1991-2015 period for which CM-SAF cloudiness satellite data are available (Stockli et al. 2017)) by focusing on clear days only (i.e., days with cloudiness lower/equal to 12.5% or 1 okta), the obtained trends are highly significant and positive with the highest value in winter. The trends result slightly lower than under all-sky conditions with the only exception of winter when, removing the cloud contribution, the trend becomes positive and significant (about +3.2% per decade).

The high-significant positive trend observed in all seasons under clear-sky conditions is in agreement with the significant reduction of air pollutant emissions and aerosol concentrations observed in Piedmont in the investigated period (Deserti et al. 2016). This suggests a relevant influence of changes in the transparency of the atmosphere on solar radiation trends. Moreover, the differences observed between all- and clear-sky conditions suggest that cloudiness variability contributed to slightly intensify the observed positive trend due to changes in the aerosol load with the only exception of winter, where cloudiness masked this signal. These hypotheses are in agreement with recent results reported in literature showing a decreasing tendency in aerosols concentrations after the 1980s (Novakov et al. 2003; Maggi et al. 2006; Vestreng et al. 2007) and a decreasing tendency of cloudiness over the Mediterranean region for all seasons with the only exception of winter where a positive tendency is observed especially in the northern part of Italy (Kotsias and Lolis 2017; Sanchez-Lorenzo et al. 2017).

Analyzing separately the plain and mountain series, the two regions show again slightly lower trends under clear-sky than under all-sky conditions (with the only exception of winter when the trend is positive and significant only under clear-sky), confirming the signal observed for the entire Piedmont region. Moreover, the comparison between the two areas shows how (differently from all-sky conditions) winter is the season during which the differences are more pronounced, with a stronger increase for low than for high elevations (about +4.1% and +2.9% per decade for the plain and mountain area, respectively) determining a positive and significant trend (+1% per decade) in the ratio series. Accordingly, the intensity of trends shows a vertical gradient of about -0.1% per decade per 100m. The intensity reduction of the winter trend with elevation is in agreement with the hypothesis that the brightening observed in Piedmont in the investigated period is mainly caused by a reduction of pollutant emissions. In winter, in fact, the boundary layer is generally rather low inhibiting the transport of polluted air masses upwards from lower regions by thermal convention (Baltensperger et al. 1991; Lugauer et al. 1998) and confining air pollutants at low levels. Therefore, high elevation areas result often scarcely influenced by low-level emissions. These areas were therefore probably less influenced than low-level areas by the reduction in the pollutant emissions that occurred in Piedmont in the investigated period. In summer, differently, the higher boundary layer causes much more similar aerosol

concentrations at low and high elevations (Magri et al. 2016).

The resulting trends and the differences obtained between low and high elevations are in agreement with the results reported in literature showing a decreasing tendency in aerosol optical depth for the considered period (Floutsi et al. 2016; Georgoulias et al. 2016) and with the fact that this trend is reported to be higher for low than for high elevations (Ruckstuhl et al. 2008; Philipona 2013).

Interestingly, the residuals of the Piedmont series from the filter (i.e. from the long-term tendency) present the minimum value (0.98 for the annual mean and 0.97 for the annual mean calculated from the September-August period) in 1992 as a consequence of the Pinatubo volcanic eruption (June 1991).

A more detailed investigation of the reasons underlying the observed trends together with the extension of this new database to the areas around the Piedmont region calls for further research.

Acknowledgement

This work was supported by the Special Project HR-CIMA within the frame of the Project of National Interest NextData.

References

Aguilar E, Auer I, Brunet M, et al (2003) Guidelines on climate metadata and homogenization. World Clim Program Data Monit WCDMP-No 53, WMO-TD No 1186 1186:50

Albrecht BA (1989) Aerosols, cloud microphysics, and fractional cloudiness. Science (80-) 245:1227–1230. doi: 10.1126/science.245.4923.1227

Auer I, Böhm R, Jurković A, et al (2005) A new instrumental precipitation dataset for the greater alpine region for the period 1800-2002. Int J Climatol 25:139–166. doi: 10.1002/joc.1135

Baltensperger U, Gäggeler HW, Jost DT, et al (1991) Continuous background aerosol monitoring with the epiphaniometer. Atmos Environ Part A, Gen Top 25:629–634. doi: 10.1016/0960-1686(91)90060-K

Boers R, Brandsma T, Pier Siebesma A (2017) Impact of aerosols and clouds on decadal trends in all-sky solar radiation over the Netherlands (1966-2015). Atmos Chem Phys 17:8081–8100. doi: 10.5194/acp-17-8081-2017

Bressi M, Cavalli F, Belis CA, et al (2016) Variations in the chemical composition of the submicron aerosol and in the sources of the organic fraction at a regional background site of the Po Valley (Italy). Atmos Chem Phys 16:12875–12896. doi: 10.5194/acp-16-12875-2016

Brunetti M, Maugeri M, Monti F, Nanni T (2006) Temperature and precipitation variability in Italy in the last two centuries from homogenised instrumental time series. Int J Climatol 26:345–381. doi: 10.1002/joc.1251

Craddock JM (1979) Methods of comparing annual rainfall records for climatic purposes. Weather 34:332–346

Deserti M, Di Giosa A, Stel F, et al (2016) La qualità dell'aria in Italia negli anni. ISPRA 68/2016

Floutsi AA, Korras-Carraca MB, Matsoukas C, et al (2016) Climatology and trends of aerosol optical depth over the Mediterranean basin during the last 12 years (2002-2014) based on Collection 006 MODIS-Aqua data. Sci Total Environ 551–552:292–303. doi: 10.1016/j.scitotenv.2016.01.192

Founda D, Kalimeris A, Pierros F (2014) Multi annual variability and climatic signal analysis of sunshine duration at a large urban area of Mediterranean (Athens). Urban Clim 10:815–830. doi: 10.1016/j.uclim.2014.09.008

Georgoulias AK, Alexandri G, Kourtidis KA, et al (2016) Differences between the MODIS Collection 6 and 5.1 aerosol datasets over the greater Mediterranean region. Atmos Environ 147:310–319. doi: 10.1016/j.atmosenv.2016.10.014

Hakuba MZ, Folini D, Sanchez-Lorenzo A, Wild M (2013) Spatial representativeness of ground-based solar radiation measurements. J Geophys Res Atmos 118:8585–8597. doi: 10.1002/jgrd.50673

Kambezidis HD, Kaskaoutis DG, Kalliampakos GK, et al (2016) The solar dimming/brightening effect over the Mediterranean Basin in the period 1979–2012. J Atmos Solar-Terrestrial Phys 150–151:31–46. doi: 10.1016/j.jastp.2016.10.006

Kazadzis S, Founda D, Psiloglou BE, et al (2018) Long-term series and trends in surface solar radiation in Athens, Greece. Atmos Chem Phys 18:2395–2411. doi: 10.5194/acp-18-2395-2018

Kotsias G, Lolis CJ (2017) A study on the total cloud cover variability over the Mediterranean region during the period 1979–2014 with the use of the ERA-Interim database. Theor Appl Climatol. doi: 10.1007/s00704-017-2276-5

Lohmann U, Feichter J (2005) Global indirect aerosol effects: a review. Atmos Chem Phys 5:715–737. doi: 1680-7324/acp/2005-5-715

Lugauer M, Baltensperger U, Furger M, et al (1998) Aerosol transport to the high Alpine sites Jungfraujoch (3454 m asl) and Colle Gnifetti (4452 m asl). Tellus, Ser B Chem Phys Meteorol 50:76–92. doi: 10.3402/tellusb.v50i1.16026

Maggi V, Villa S, Finizio A, et al (2006) Variability of anthropogenic and natural compounds in high altitude-high accumulation alpine glaciers. Hydrobiologia 562:43–56. doi: 10.1007/s10750-005-1804-y

Magri T, Angelino E, Grosa M, et al (2016) Riscaldamento domestico a legna e qualità dell'aria nelle regioni dell'arco alpino. ISPRA 68/2016

Manara V, Beltrano MC, Brunetti M, et al (2015) Sunshine duration variability and trends in Italy from homogenized instrumental time series (1936-2013). J Geophys Res 120:. doi: 10.1002/2014JD022560

Manara V, Brunetti M, Celozzi A, et al (2016a) Detection of dimming/brightening in Italy from

homogenized all-sky and clear-sky surface solar radiation records and underlying causes (1959-2013). Atmos Chem Phys 16:11145–11161. doi: 10.5194/acp-16-11145-2016

Manara V, Brunetti M, Maugeri M, et al (2017a) Homogenization of a surface solar radiation dataset over Italy. In: AIP Conference Proceedings

Manara V, Brunetti M, Maugeri M, et al (2017b) Sunshine duration and global radiation trends in Italy (1959-2013): To what extent do they agree? J Geophys Res 122:. doi: 10.1002/2016JD026374

Manara V, Brunetti M, Maugeri M (2016b) Reconstructing sunshine duration and solar radiation long-term evolution for Italy: a challenge for quality control and homogenization precedures. In: 14th IMEKO TC10 Workshop Technical Diagnostics - New Perspectives in Measurements, Tools and Techniques for system's reliability, maintainability and safety. pp 13–18

Manara V, Brunetti M, Maugeri M, et al (2017c) Homogenization of a surface solar radiation dataset over Italy. In: Radiation processes in the atmosphere And Ocean (IRS 2016) - AIP Conference proceeding. AIP Publishing, pp 90004-1-90004–4

Marty C, Philipona R, Frøhlich C, Ohmura A (2002) Altitude dependence of surface radiation fluxes and cloud forcing in the alps: Results from the alpine surface radiation budget network. Theor Appl Climatol 72:137–155. doi: 10.1007/s007040200019

Mateos D, Sanchez-Lorenzo A, Antón M, et al (2014) Quantifying the respective roles of aerosols and clouds in the strong brightening since the early 2000s over the Iberian Peninsula. J Geophys Res Atmos 119:10382–10393. doi: 10.1002/2014JD022076

Norris JR, Wild M (2007) Trends in aerosol radiative effects over Europe inferred from observed cloud cover, solar "dimming" and solar "brightening." J Geophys Res Atmos 112:1–13. doi: 10.1029/2006JD007794

Novakov T, Ramanathan V, Hansen JE, et al (2003) Large historical changes of fossil-fuel black carbon aerosols. Geophys Res Lett 30:1324. doi: 10.1029/2002GL016345

Pfeifroth U, Sanchez-Lorenzo A, Manara V, et al (2018) Trends and Variability of Surface Solar Radiation in Europe Based On Surface- and Satellite-Based Data Records. J Geophys Res Atmos 123:1735–1754. doi: 10.1002/2017JD027418

Philipona R (2013) Greenhouse warming and solar brightening in and around the Alps. Int J Climatol 33:1530–1537. doi: 10.1002/joc.3531

Ramanathan V, Crutzen PJ, Kiehl JT, Rosenfeld D (2001) Aerosols, Climate, and the Hydrological Cycle. Science (80-) 294:2119–2124. doi: 10.1126/science.1064034

Ruckstuhl C, Philipona R, Behrens K, et al (2008) Aerosol and cloud effects on solar brightening and the recent rapid warming. Geophys Res Lett 35:. doi: 10.1029/2008GL034228

Sanchez-Lorenzo A, Enriquez-Alonso A, Calbó J, et al (2017) Fewer clouds in the Mediterranean: Consistency of observations and climate simulations. Sci Rep 7:1–10. doi: 10.1038/srep41475

Sanchez-Lorenzo A, Wild M (2012) Decadal variations in estimated surface solar radiation over Switzerland since the late 19th century. Atmos Chem Phys 12:8635–8644. doi: 10.5194/acp-12-8635-2012

Sanchez-Lorenzo A, Wild M, Brunetti M, et al (2015) Reassessment and update of long-term trends in downward surface shortwave radiation over Europe (1939-2012). J Geophys Res Atmos 120:9555–9569. doi: 10.1002/2015JD023321

Sanroma E, Palle E, Sanchez-Lorenzo A (2010) Long-term changes in insolation and temperatures at different altitudes. Environ Res Lett 5:24006. doi: 10.1088/1748-9326/5/2/024006

Schwarz M, Folini D, Hakuba MZ, Wild M (2017) Spatial Representativeness of Surface-Measured Variations of Downward Solar Radiation. J Geophys Res Atmos 122:13,319-13,337. doi: 10.1002/2017JD027261

Sen PK (1968) Estimates of the Regression Coefficient Based on Kendall's Tau. J Am Stat Assoc 63:1379–1389. doi: 10.1080/01621459.1968.10480934

Sneyers R (1992) On the use of statistical analysis for the objective determination of climate change. Meteorol Zeitschrift 1:247–256

Stanhill G (1983) The distribution of global solar radiation over the land surfaces of the Earth. Sol Energy 31:95–104

Stephens GL, Li J, Wild M, et al (2012) An update on Earth's energy balance in light of the latest global observations. Nat Geosci 5:691–696. doi: 10.1038/ngeo1580

Stockli R, Duguay-Tetzlaff A, Bojanowski J, et al (2017) CM SAF ClOud Fractional Cover dataset from METeosat First and Second Generation - Edition 1 (COMET Ed. 1). Satell Appl Facil Clim Monit. doi: 10.5676/EUM_SAF_CM/CFC_METEOSAT/V001

Suter S, Konzelmann T, Mühlhäuser C, et al (2006) SwissMetNet - The new automatic meteorological network of Switzerland: Transition from old to new network, data management and first results. Proc 4th Int Conf Exp with Autom Weather Station (4th ICEAWS)

Tang W, Yang K, Qin J, et al (2017) A revisit to decadal change of aerosol optical depth and its impact on global radiation over China. Atmos Environ 150:106–115. doi: http://dx.doi.org/10.1016/j.atmosenv.2016.11.043

Theil H (1950) A rank-invariant method of linear and polynomical regression analysis. In: Proceedings of the Royal Academy of Sciences. pp 386–392

Turnock ST, Spracklen D V., Carslaw KS, et al (2015) Modelled and observed changes in aerosols and surface solar radiation over Europe between 1960 and 2009. Atmos Chem Phys 15:9477–9500. doi: 10.5194/acp-15-9477-2015

Twomey SA, Piepgrass M, Wolfe TL (1984) An assessment of the impact of pollution on global cloud albedo. Tellus 36B:356–366. doi: 10.1111/j.1600-0889.1984.tb00254.x

Vestreng V, Myhre G, Fagerli H, et al (2007) Twenty-five years of continuous sulphur dioxide emission reduction in Europe. Atmos Chem Phys 7:3663–3681. doi: 10.5194/acp-7-3663-2007

Wild M (2016) Decadal changes in radiative fluxes at land and ocean surfaces and their relevance for global warming. Wiley Interdiscip Rev Clim Chang 7:91–107. doi: 10.1002/wcc.372

Wild M (2009) Global dimming and brightening: A review. J Geophys Res 114:D00D16. doi: 10.1029/2008JD011470

Wild M, Folini D, Henschel F, et al (2015) Projections of long-term changes in solar radiation based on CMIP5 climate models and their influence on energy yields of photovoltaic systems. Sol Energy 116:12–24. doi: 10.1016/j.solener.2015.03.039

	Year	Winter	Spring	Summer	Autumn
Piedmont	**2.5±0.9**	-	2.6±1.3	**2.7±1.2**	**4.0±1.4**
Plain	**2.6±0.8**	-	3.1±1.5	**2.6±1.2**	**4.7±1.8**
Mountain	**2.3±0.8**	-	2.4±1.1	**2.8±1.2**	**3.9±1.6**
Plain/Mountain	0.4±0.2	-	**0.7±0.3**	+	+
Variation of the trend intensity for an increase in elevation of 100m	**-0.03±0.01**	+	**-0.07±0.01**	+	-

[a]Values are expressed in % per decade and they are provided together with an estimation of their standard deviations (half widths of 68% confidence intervals). Values are shown in roman for significance level of $0.05<p\leq0.1$ and in bold for a significance level of $p\leq0.05$. For non-significant trends, only the sign of the slope is given. The significance of the trends is evaluated with the Mann-Kendall non parametric test while trends are estimated with the Theil-Sen method.

Table 1

Table caption

Table 1: Annual and seasonal trends obtained for the Piedmont region, and for the plain and mountain areas under all-sky conditions. Annual and seasonal trends of the ratio between plain and mountain regional series are shown too, together with annual and seasonal variation of the intensity of trend every 100m of increase in elevation[a]

Figure captions

Fig. 1*: a) Spatial distribution of stations and grid-points. Colors indicate data sources. Blue: Piedmont regional service (Arpa – 60 series). Yellow: National Agrometeorological database (BDAN – 2 series). Green: Italian Air Force (AM – 1 series). Orange: MeteoSwiss (11 series). Stations/grid-points located in the plain area (elevation lower than or equal to 600m) are represented with a dot, while those located in the mountain area (elevation higher than 600m) are represented with a triangle; b) Number of stations as a function of the elevation; c) Temporal evolution of the number of available records per year considering the entire dataset (solid line), only the stations located in the plain area (dashed line) and only the stations located in the mountain area (dotted line)*

Fig. 2*: Average annual $E_{g\downarrow}$ anomaly series, plotted together with an 11-year window, 3-year standard deviation Gaussian low-pass filter, before (black line) and after (red line) the homogenization procedure. The blue line represents the mean annual adjustment series obtained by calculating the annual average of the adjustments over all series*

Fig. 3*: Average annual and seasonal $E_{g\downarrow}$ anomaly series obtained under all-sky conditions for the Piedmont region plotted together with an 11-year window, 3-year standard deviation Gaussian low-pass filter. The series are expressed as relative deviations from the 1990-2016 mean. Note that the y-axis in the annual plot is shown with an expanded scale and that the annual series is the same of the red line reported in Figure 2*

Fig. 4*: Annual and seasonal trend (expressed in % per decade) for each grid-point obtained under all-sky conditions. Dots and triangles are used for those grid-points that are representative of a plain (weighted elevation lower than or equal to 600m) and mountain (weighted elevation higher than 600m) area, respectively. A big symbol is used when the trend has p-value ≤ 0.1 while a small symbol is used when the trend is not significant. p-values are estimated by means of the Mann-Kendall test*

Fig. 5*: Annual and seasonal trend (expressed in % per decade) for each grid-point in relation to elevation obtained under all-sky conditions. A black dot is used when the trend has p-value ≤ 0.1 while a grey dot is used when the trend is not significant. p-values are estimated by means of the Mann-Kendall test*

Fig. 6*: Comparison between the annual Piedmont plain (red line – 1990-2016 period) and the annual northwest Italy (black line – 1959-2013 period) relative anomaly series. The anomalies are calculated with respect to the 1990-2004 period*

Fig. 7*: Average annual and seasonal* $E_{g\downarrow}$ *anomaly series, over the 1991-2015 period, obtained under clear-sky conditions for the Piedmont region plotted together with an 11-year window, 3-year standard deviation Gaussian low-pass filter (red lines). The filters under all-sky conditions are shown too (black lines). The series are expressed as relative deviations from the 1991-2015 mean. Note that the y-axis in the annual plot is shown with an expanded scale*

Fig. 8*: Winter trend (expressed in % per decade) for each grid-point in relation to elevation obtained under clear-sky conditions. A black dot is used when the trend has p-value* ≤ 0.1 *while a grey dot is used when the trend is not significant. p-values are estimated by means of the Mann-Kendall test*

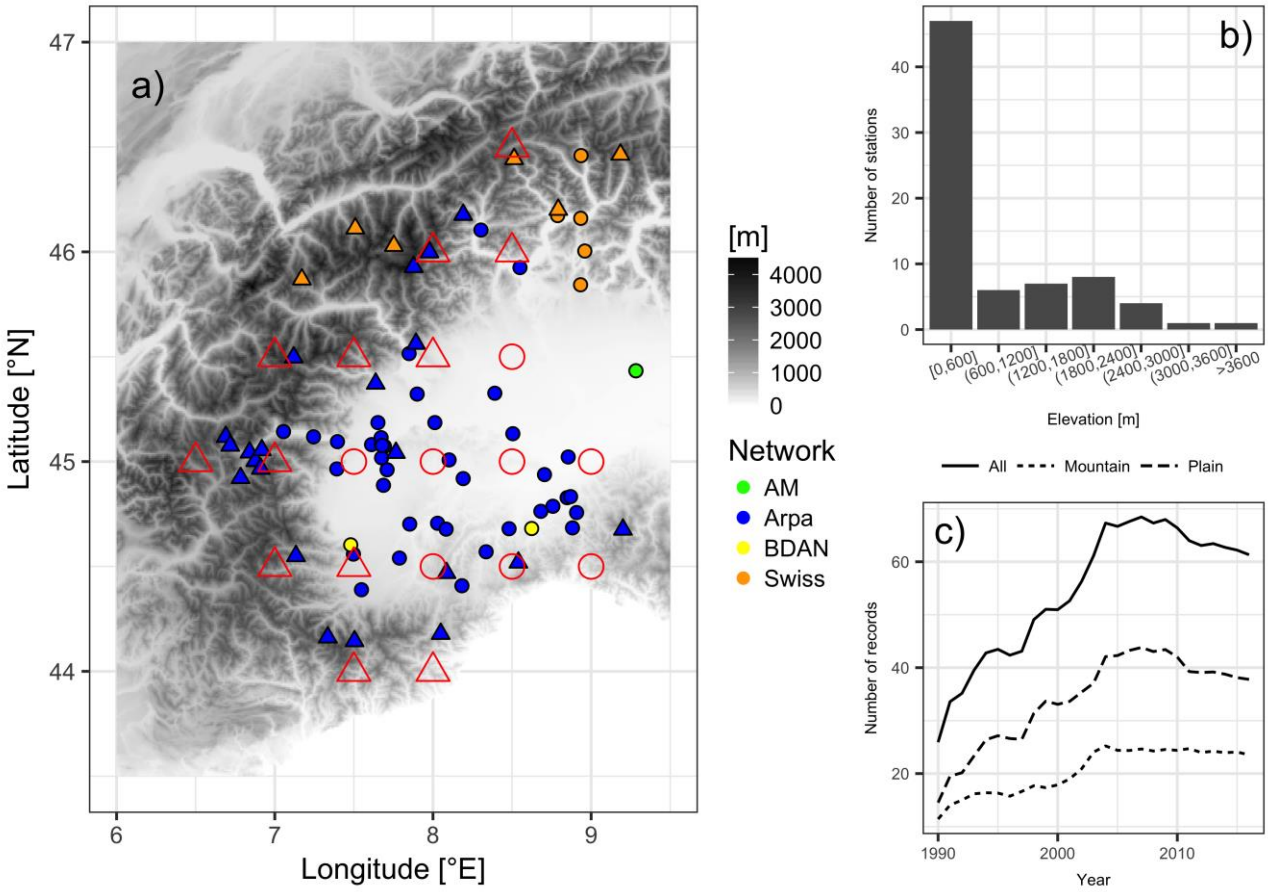
a)
Latitude [°N]
Longitude [°E]
47
46
45
44
6
7
8
9
[m]
4000
3000
2000
1000
0
Network
AM
Arpa
BDAN
Swiss
b)
Number of stations
Elevation [m]
[0,600]
(600,1200]
(1200,1800]
(1800,2400]
(2400,3000]
(3000,3600]
>3600
All
Mountain
Plain
c)
Number of records
Year
1990
2000
2010

Figure 1

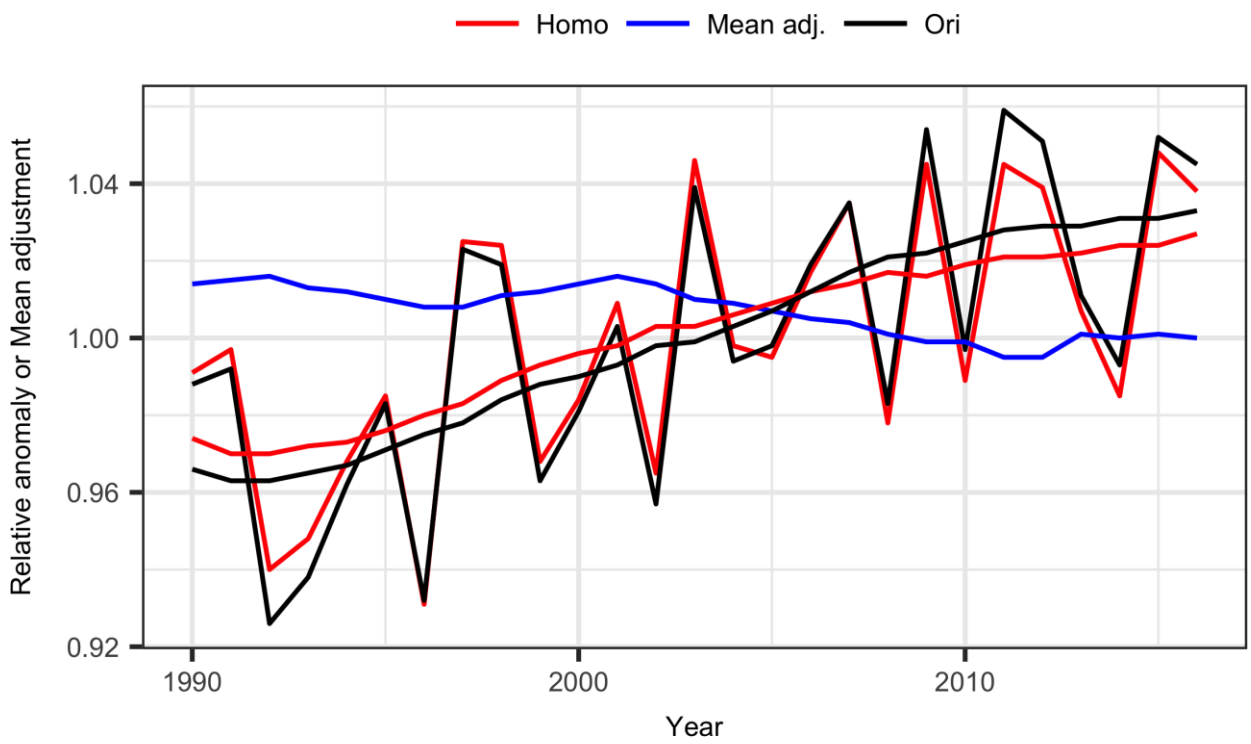
Homo
Mean adj.
Ori
Relative anomaly or Mean adjustment
1.04
1.00
0.96
0.92
1990
2000
2010
Year

Figure 2

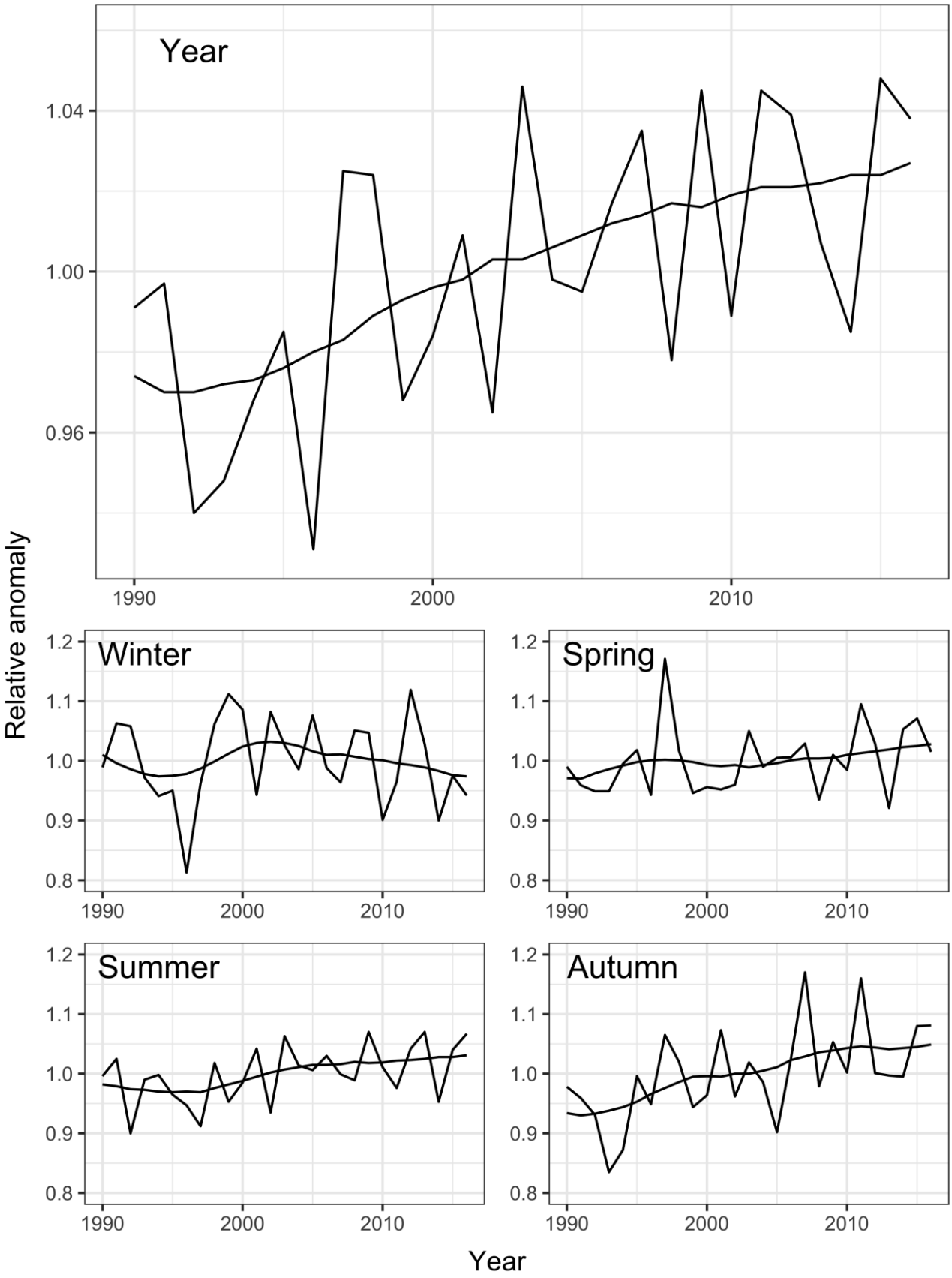
Year
1.04
1.00
0.96
1990
2000
2010
Relative anomaly
Winter
Spring
Summer
Autumn
1.2
1.1
1.0
0.9
0.8
Year

Figure 3

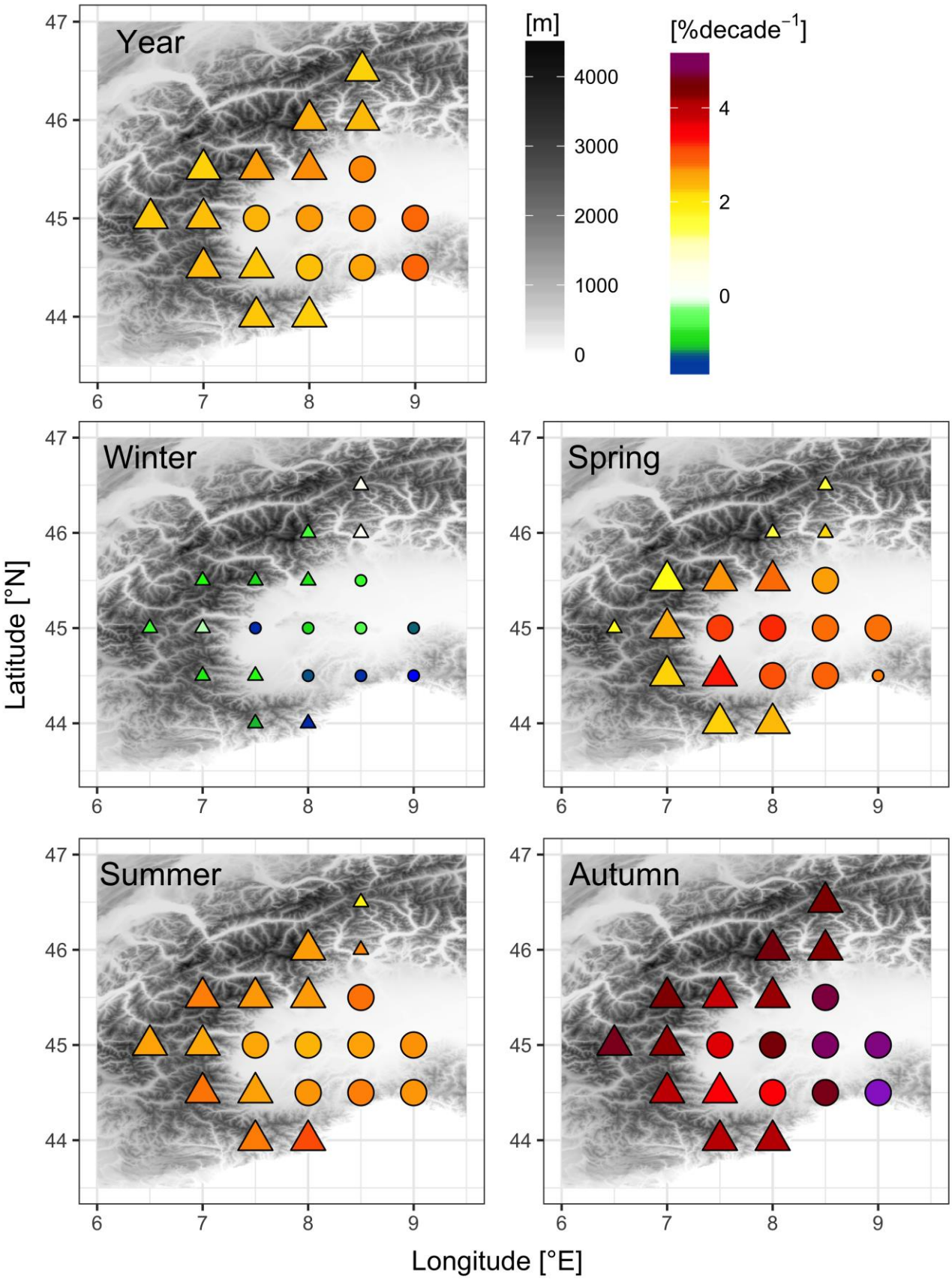
Year
Winter
Spring
Summer
Autumn
[m]
4000
3000
2000
1000
0
[%decade^{-1}]
4
2
0
Latitude [°N]
Longitude [°E]
47
46
45
44
6
7
8
9

Figure 4

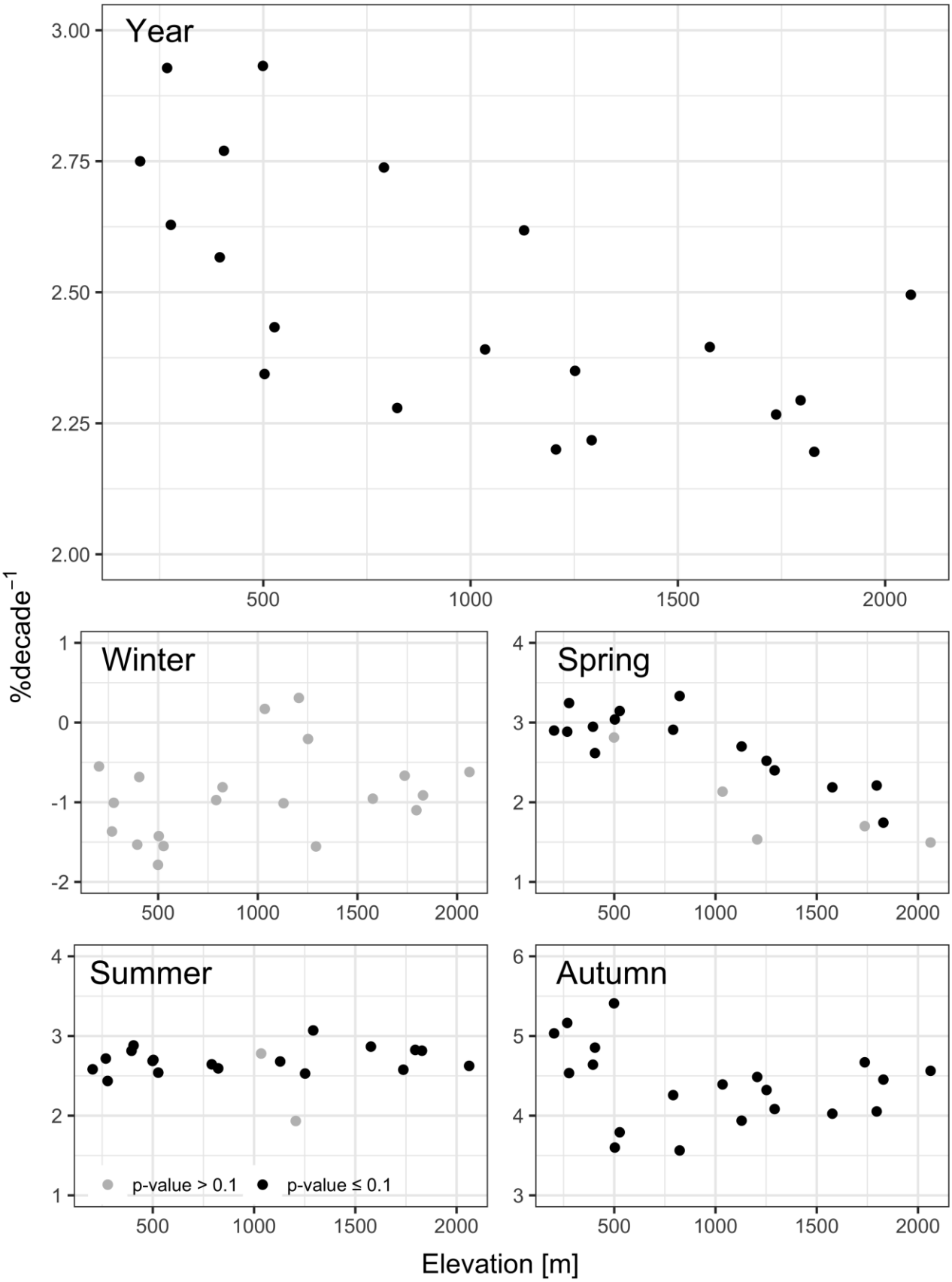
Year
Winter
Spring
Summer
Autumn
%decade^{-1}
Elevation [m]
p-value > 0.1
p-value ≤ 0.1

Figure 5

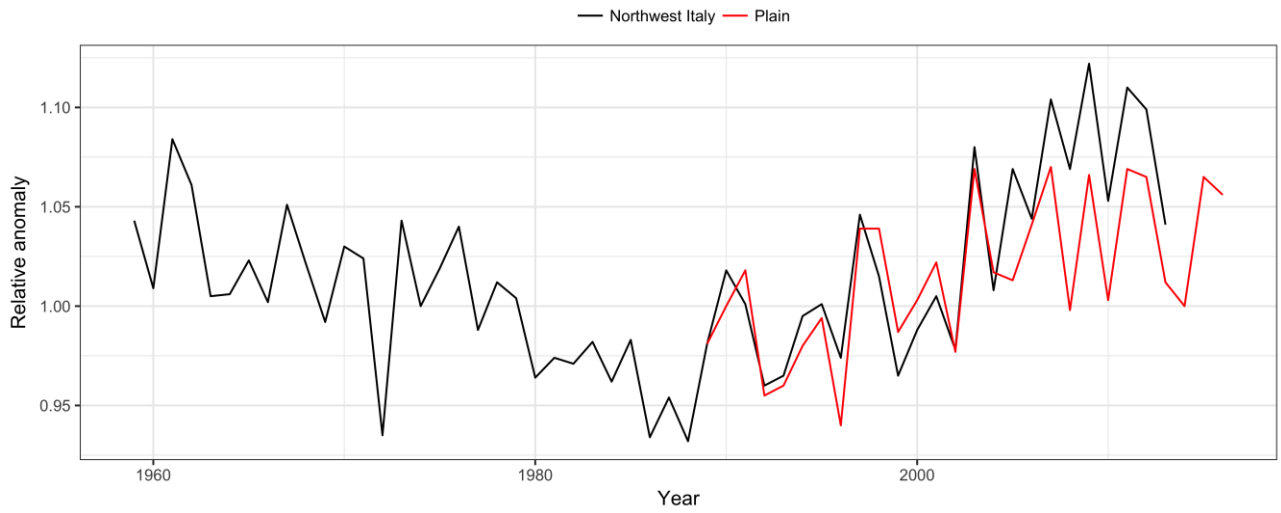
Northwest Italy
Plain
Relative anomaly
1.10
1.05
1.00
0.95
1960
1980
2000
Year

Figure 6

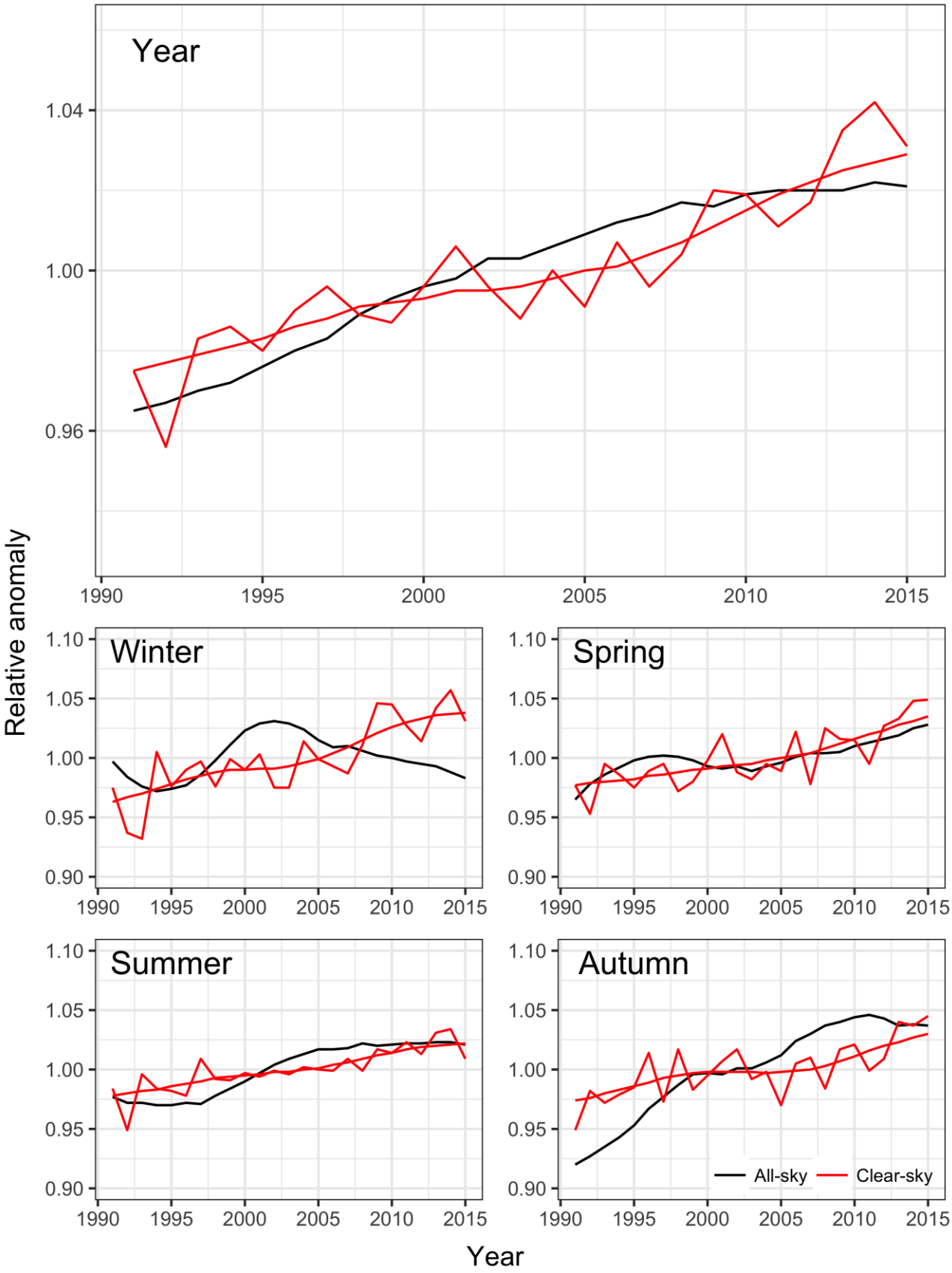
Year
Winter
Spring
Summer
Autumn
Relative anomaly
Year
All-sky
Clear-sky
1.04
1.00
0.96
1.10
1.05
0.95
0.90
1990
1995
2000
2005
2010
2015

Figure 7

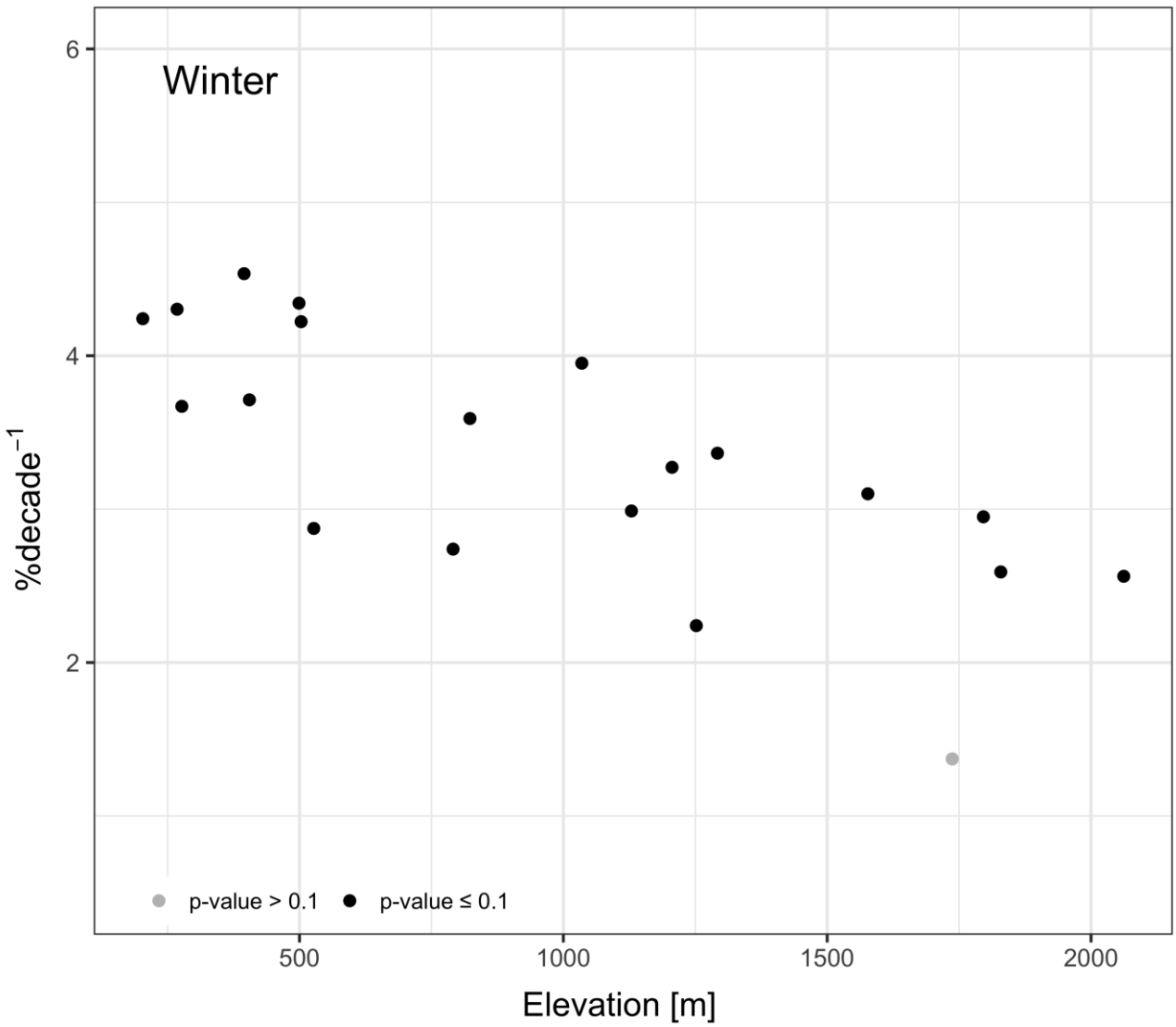
Winter
6
4
2
%decade^{-1}
p-value > 0.1
p-value ≤ 0.1
500
1000
1500
2000
Elevation [m]

Figure 8